MET.O.14

METEOROLOGICAL OFFICE
BOUNDARY LAYER RESEARCH BRANCH
TURBULENCE & DIFFUSION NOTE

T.D.N. No. 89

Stratification effects in boundary layer flow over hills.

by

R.I.Sykes

November 1977

MFT

Stratification effects in boundary layer flow over hills

R I Sykes

Meteorological Office, Bracknell

Abstract

The triple-deck analysis of boundary layer flow over topography is extended to include the effects of stable stratification in the free-stream. Analysis of the linearised three-dimensional flow shows that gravity waves generated in the outer region have a significant influence on the flow in the boundary layer due to the interactive nature of the triple-deck structure. Numerical solution of the two-dimensional non-linear equations shows the inhibition of separation by the stratificiation, and also gives larger amplitudes of the generated gravity waves than would be expected from the linearised theory.

1. Introduction

In a recent paper, Smith, Sykes, and Brighton (1977) developed a three-dimensional theory of boundary layer flow over topography and on the 'triple-deck' analysis, see Stewartson (1974). This analysis is restricted to particular length and height scales of topography, but these are in fact very important scales for the boundary layer dynamics. The triple-deck analysis determines the size of surface features which induce an interaction between the boundary layer and the free stream, and also determines the nature of the interaction. The effects of topography were first analysed for two-dimensional flow by F T Smith (1973), and for three-dimensional pipeflow by F T Smith (1976).

Although the flow described by Smith, Sykes, and Brighton (hereafter referred to as (A)) is a laminar flow, an understanding of such problems is an important preliminary to the study of atmospheric flow over hills. The atmosphere is usually stably stratified outside the boundary layer, and topography of suitable horizontal dimensions, roughly 1 - 10 km, will generate internal gravity waves. Most theoretical treatments of stratified flow over topography, eg Queney (1949), Scorer (1953), Bretherton (1969), assume an inviscid fluid, and attention has been concentrated on investigating the effects of vertical variation of temperature gradient and velocity. However, since most hills on scales shorter than 10 km are smaller than the depth of the boundary layer (i.e. typically less than a few hundred metres high), the boundary layer dynamics might be expected to play a significant role.

In this paper, the effects of stratification are included in the triple-deck interaction on the assumption that buoyancy effects are only appreciable in the flow outside the boundary layer. For typical values of atmospheric parameters, specifying a constant eddy viscosity of 5 $m^2 s^{-1}$, this will be shown to be a reasonable assumption.

The next section describes the analysis of the stratified upper deck problem, and the matching with the boundary layer solution. Section 3 presents the linearised solution of the three-dimensional problem, valid for very small hills. Section 4 describes a numerical scheme for the solution of the two-dimensional non-linear problem, and Section 5 presents some numerical results. Section 6 discusses the forces due to the presence of the topography.

2. Triple-deck analysis with stratified free-stream

The flow under consideration is illustrated in figure 1, and consists of a uniform flow of speed U_0 in the x-direction above a no-slip boundary. The hill has lengths of order L in both the x^* and y^*-directions, and the fluid has kinematic viscosity ν. These three quantities define a Reynolds number $Re = \frac{U_0 L}{\nu}$. The geometry is identical to that in (A), where it was shown that $\varepsilon = Re^{-1/5}$ is the important small parameter for the triple-deck interaction. The boundary layer must have a depth of order εL, and the height of the hill is $O(\varepsilon^2 L)$. The boundary layer scale, $z^* = O(\varepsilon L)$ then becomes the main deck, with a lower deck in which $z^* = O(\varepsilon^2 L)$, and an upper deck with $z^* = O(L)$, these three scales forming an interactive flow system. The effects of stratification

can be incorporated into this structure without changing the nature of the interaction, provided the buoyancy is only important in the upper deck.

The dimensionless number associated with the stratification is written as an inverse internal Froude number $S = \frac{NL}{U_0}$, where N is the Brunt - Vaisala frequency $\left[-\frac{g}{\bar{\rho}}\frac{d\rho_0}{dz^*}\right]^{1/2}$. Here g is the acceleration due to gravity, $\bar{\rho}$ is the mean density, and $\frac{d\rho_0}{dz^*}$ is the undisturbed density gradient in the free-stream. We assume $\bar{\rho}$ is a constant since we will be making the Boussinesq approximation later, i.e. the variations in density are much smaller than $\bar{\rho}$. We show below that $S = O(1)$ is the required magnitude of the inverse Froude number.

Before proceeding, some typical parameter values are presented. We assume an eddy viscosity of $5 m^2 s^{-1}$, and a boundary layer depth of 300 m. These values represent typical atmospheric values, although it must be remembered that the turbulent boundary layer has a significantly different detailed structure. For a geostrophic wind of 10 ms^{-1}, this gives $\varepsilon \triangleq 0.2$, so the length of the topography is of order 1.5 km, and its height of order 60 m. If N is taken to be $10^{-2}\ s^{-1}$, this implies S = 1.5.

The Boussinesq equations of motion are

$$u^*\frac{\partial u^*}{\partial x^*} + v^*\frac{\partial u^*}{\partial y^*} + w^*\frac{\partial u^*}{\partial z^*} = -\frac{\partial p}{\partial x^*} + \nu\nabla^2 u^* \qquad (2.1)$$

$$u^*\frac{\partial v^*}{\partial x^*} + v^*\frac{\partial v^*}{\partial y^*} + w^*\frac{\partial v^*}{\partial z^*} = -\frac{\partial p}{\partial y^*} + \nu\nabla^2 v^* \qquad (2.2)$$

$$u^*\frac{\partial w^*}{\partial x^*} + v^*\frac{\partial w^*}{\partial y^*} + w^*\frac{\partial w^*}{\partial z^*} = -\frac{\partial p}{\partial z^*} - \frac{g\rho^*}{\bar{\rho}} + \nu\nabla^2 w^* \qquad (2.3)$$

$$u^*\frac{\partial \rho^*}{\partial x^*} + v^*\frac{\partial \rho^*}{\partial y^*} + w^*\frac{\partial \rho^*}{\partial z^*} = K\nabla^2\rho^* \qquad (2.4)$$

$$\frac{\partial u^*}{\partial x^*} + \frac{\partial v^*}{\partial y^*} + \frac{\partial w^*}{\partial z^*} = 0 \qquad (2.5)$$

where ρ^* is the density perturbation, K is the thermal diffusivity, and an asterisk denotes a dimensional quantity.

Scale the variables, $(x^*, y^*) = L(x, y)$,

$(u^*, v^*, w^*) = U_0(u, v, w)$, and $p^* = U_0^2 p$.

The basic density $\frac{d\rho_0}{dz^*}$ can be eliminated from (2.3) by subtracting out the hydrostatic pressure P_0^*, defined by $\frac{dP_0^*}{dz^*} = -g\rho_0$, hence the buoyancy term in term in (2.3) can be written as $-\frac{g}{\bar{\rho}}(\rho^* - \rho_0(z^*))$. So if we define the dimensionless density $\rho = \frac{\rho^* - \rho_0}{-L\frac{d\rho_0}{dz^*}}$, then the buoyancy term finally becomes $LN^2\rho$.

The lower deck scale Z is defined by $z^* = \varepsilon^2 L Z$, thus the lower deck density equation (2.4) in dimensionless variables is

$$u\frac{\partial\rho}{\partial x} + v\frac{\partial\rho}{\partial y} + \varepsilon^{-2}w\frac{\partial\rho}{\partial Z} - w = \kappa\left(\frac{\partial^2\rho}{\partial x^2} + \frac{\partial^2\rho}{\partial y^2} + \varepsilon^{-4}\frac{\partial^2\rho}{\partial Z^2}\right) \quad (2.6)$$

It was pointed out in (A) that in the lower deck $u = O(\varepsilon)$, and $w = O(\varepsilon^3)$, hence (2.6) shows $\rho = O(\varepsilon^2)$ provided the Prandtl number ν/κ is $O(1)$. The buoyancy term in the vertical momentum equation is $-S^2\rho$, so if $S = O(1)$ this term is $O(\varepsilon^2)$. However $\frac{\partial p}{\partial Z} = O(1)$ since $p = O(\varepsilon^2)$ throughout the flow, hence the lower deck momentum equations are unchanged.

A similar argument, using the velocity magnitudes from (A), shows that the main deck equations are unchanged.

We therefore present the lower and main deck results directly from (A)

Main deck

We expand the solutions

$$\begin{aligned} u &= u_B(z) + \varepsilon u_1 + O(\varepsilon^2) \\ v &= \varepsilon^2 v_1 + O(\varepsilon^3) \\ w &= \varepsilon^2 w_1 + O(\varepsilon^3) \\ p &= \varepsilon^2 p_1 + O(\varepsilon^3) \end{aligned} \quad (2.7)$$

where $Z = \frac{z^*}{\varepsilon L}$, and $u_B(z)$ is the upstream dimensionless boundary layer profile.

The main deck solution is therefore

$$\begin{aligned} u_1 &= A(x,y)\, u_B'(z) \\ w_1 &= -\frac{\partial A}{\partial x}\, u_B(z) \\ v_1 &= D(x,y)/u_B(z) \\ p_1 &= P(x,y) \end{aligned} \qquad (2.8)$$

where $\frac{\partial D}{\partial x} = -\frac{\partial P}{\partial y}$, and A and P are to be determined.

Lower deck

Define

$$\begin{aligned} u &= \varepsilon U + O(\varepsilon^2) \\ v &= \varepsilon V + O(\varepsilon^2) \\ w &= \varepsilon^3 W + O(\varepsilon^4) \\ p &= \varepsilon^2 P(x,y) + O(\varepsilon^3) \end{aligned} \qquad (2.9)$$

Then the leading terms in the equations of motion are

$$\begin{aligned} U\frac{\partial U}{\partial x} + V\frac{\partial U}{\partial y} + W\frac{\partial U}{\partial Z} &= -\frac{\partial P}{\partial x} + \frac{\partial^2 U}{\partial Z^2} \\ U\frac{\partial V}{\partial x} + V\frac{\partial V}{\partial y} + W\frac{\partial V}{\partial Z} &= -\frac{\partial P}{\partial y} + \frac{\partial^2 V}{\partial Z^2} \\ \frac{\partial U}{\partial x} + \frac{\partial V}{\partial y} + \frac{\partial W}{\partial Z} &= 0 \end{aligned} \qquad (2.10)$$

with boundary conditions

$$\begin{aligned} &U = V = W = 0 \quad \text{on} \quad Z = h(x,y), \text{the lower boundary} \\ &\left.\begin{aligned} U &\sim Z + A(x,y) \\ V &\sim D(x,y)/Z \\ W &\sim -Z\frac{\partial A}{\partial x} \end{aligned}\right\} \quad \text{as } Z \to \infty \end{aligned} \qquad (2.11)$$

Here we have assumed that $u_B'(0) = 1$, since other values of the undisturbed skin friction are obtained by re-scaling the variables, as shown in (A).

Stratified upper deck

The displacement $A(x,y)$ at the top of the boundary layer induces a pressure field in the upper deck, which is communicated to the surface and drives the lower deck flow. Thus the upper deck solution provides the relation between the streamline displacement, $A(x,y)$, and the pressure $P(x,y)$.

The velocity scales are unchanged by stratification if $S = O(1)$, so we expand the variables as

$$\begin{aligned} u &= 1 + \varepsilon^2 u_1 + O(\varepsilon^3) \\ v &= \varepsilon^2 v_1 + O(\varepsilon^3) \\ w &= \varepsilon^2 w_1 + O(\varepsilon^3) \\ p &= \varepsilon^2 p_1 + O(\varepsilon^3) \\ \rho &= \varepsilon^2 \rho_1 + O(\varepsilon^3) \end{aligned} \qquad (2.12)$$

Then substituting in the Navier - Stokes equations (2.1) - (2.5) gives

$$\begin{aligned} \frac{\partial u_1}{\partial x} &= -\frac{\partial p_1}{\partial x} \\ \frac{\partial v_1}{\partial x} &= -\frac{\partial p_1}{\partial y} \\ \frac{\partial w_1}{\partial x} &= -\frac{\partial p_1}{\partial z} - S^2 \rho_1 \\ \frac{\partial \rho_1}{\partial x} &= w_1 \\ \frac{\partial u_1}{\partial x} &+ \frac{\partial v_1}{\partial y} + \frac{\partial w_1}{\partial z} = 0 \end{aligned} \qquad (2.13)$$

where $z = z^*/L$.

Equations (2.13) can be combined to give

$$\nabla^2 \frac{\partial^2 p_1}{\partial x^2} + S^2 \left(\frac{\partial^2 p_1}{\partial x^2} + \frac{\partial^2 p_1}{\partial y^2} \right) = 0 \qquad (2.14)$$

The boundary conditions at $z = 0$ on (2.13) are obtained by matching with the top of the main deck, giving

$$p_1(x, y, 0) = P(x, y) \qquad (2.15)$$

and

$$w_1(x, y, 0) = -\frac{\partial A}{\partial x}$$

i.e.

$$\left.\frac{\partial p_1}{\partial z}\right|_{z=0} + S^2 \left. p_1 \right|_{z=0} = \frac{\partial^2 A}{\partial x^2} \qquad (2.16)$$

Define the Fourier transform $\overline{p_1}(k, l, z) = \int_{-\infty}^{\infty} \int_{-\infty}^{\infty} p_1(x, y, z)\, e^{-i(kx + ly)}\, dx\, dy$

then (2.14) and (2.15) give

$$\overline{p_1} = \overline{P}(k, l)\, e^{imz}$$

where $m^2 = \dfrac{(k^2 + l^2)(S^2 - k^2)}{k^2}$, and the overbar denotes a Fourier transform.

If $|k| > S$, then m is imaginary, and the decaying mode must be chosen, i.e.

$$m = \frac{i}{k}(k^2+\ell^2)^{1/2}(k^2-S^2)^{1/2}, \quad |k| > S \qquad (2.17)$$

When $|k| < S$, the solutions are wavelike in the vertical, and the mode which transports energy upwards must be chosen.

This is most easily seen by transforming into the frame of the fluid in the free-stream, i.e. the lower boundary is now moving with velocity $(-1, 0, 0)$. The full dispersion relation is then

$$\omega = \pm \frac{S(k^2+\ell^2)^{1/2}}{(k^2+\ell^2+m^2)^{1/2}}$$

where ω is the wave frequency and the sign is to be determined. The vertical group velocity of this wave is

$$\frac{\partial \omega}{\partial m} = -\operatorname{sgn}(\omega)\, m\, \frac{S(k^2+\ell^2)^{1/2}}{(k^2+\ell^2+m^2)^{1/2}}$$

Since we are seeking a steady solution in the frame of the lower boundary, the waves must have a phase speed equal to -1, i.e. $\omega = -k$; thus the sign of ω is opposite to that of k. If we now demand that $\frac{\partial \omega}{\partial m} > 0$, then $\operatorname{sgn}(m) = \operatorname{sgn}(k)$. Thus

$$m = (k^2+\ell^2)^{1/2}(S^2-k^2)^{1/2}/k \quad , \quad |k| < S \qquad (2.18)$$

Using (2.13) to relate $\overline{\rho}_1$ to $\overline{A}$ at $z=0$, and the second boundary condition (2.16),

$$-S^2\overline{A} + im\overline{P} = -k^2\overline{A}$$

i.e.

$$\overline{A} = -\frac{im\overline{P}}{k^2-S^2} \qquad (2.19)$$

where m is determined by (2.17), (2.18).

Thus the problem is to solve the lower deck equations (2.10) subject to the boundary conditions (2.11) together with relation (2.19). The linearised three-dimensional solution is described in the next section, and some two-dimensional numerical solutions are presented in section 5.

3. Linearised solution (three-dimensional)

If we assume the hill is very small, i.e. $h(x,y) = h_0 F(x,y)$ with $h_0 \ll 1$, the equations (2.10) can be linearised about the basic state, and then solved by Fourier transforms. This approach is identical to the method used in (A), and the details are ommited.

We expand $U = Z + h_0 \hat{U}$, $(V, W, A, P) = h_0 (\hat{V}, \hat{W}, \hat{A}, \hat{P})$. The only difference in the analysis is the relation between $\hat{A}$ and $\hat{P}$, so the result is simply stated here. In Fourier transform space, we find

$$\overline{\hat{P}} = -\frac{k^2 \overline{F}}{\{\theta^{-4/3}(ik)^{1/3}(k^2+\ell^2) - imk^2/(k^2-S^2)\}}$$

where $\theta = (-3Ai'(0))^{3/4}$, Ai is the Airy function, and $(ik)^{1/3}$ is defined with a branch cut along the positive imaginary k-axis, and $-\frac{3\pi}{2} < \arg k \leq \frac{\pi}{2}$. The value of m is determined by equations (2.17), (2.18).

Expressions for the other fields are obtained as described in (A), and we now present some results for $S=3$ obtained using the Fast Fourier Transform for the numerical calculations. Figure 2 shows the pressure field for flow over the hill

$$F(x,y) = \begin{cases} \cos^2\left(\frac{\pi}{2}(x^2+y^2)^{\frac{1}{2}}\right), & x^2+y^2 \leq 1 \\ 0 & \text{, otherwise} \end{cases} \qquad (3.1)$$

The local values around the hill are very similar to the homogeneous case, but downstream the wave structure is evident. The asymptotic behaviour is also quite different. An analysis along the same lines as (A) gives

$$\hat{P}(x,y) \sim -\frac{S\,x}{(x^2+y^2)^{3/2}} \quad \text{as} \quad x^2+y^2 \to \infty$$

which is a slower decay than the homogeneous problem.

Figure 3 shows the streamwise skin friction perturbation $\left.\frac{\partial \hat{u}}{\partial z}\right|_{z=0}$. The reduction in the magitude of the minimum at the rear of the hill, from the homogeneous value of -0.42 to -0.21 by the stratification, implies that separation will be inhibited. The waves downstream appear to be restricted laterally to a corridor as in the homogeneous case. Asymptotic analysis confirms the existence of a corridor with the same width as the hill, and $\frac{\partial \hat{u}}{\partial z}$ decaying like $x^{-4/3}$ inside this corridor. The regions of accelerated surface fluid at the outer edges of and outside the corridor are also removed by the stratification.

There is also a corridor effect in the streamline displacement, $-\hat{A}(x,y)$, illustrated in Figure 4. The gravity waves are particularly obvious here, extending downstream inside the corridor. The apparent upstream corridor is a result of the periodic boundary conditions; in the isolated case there is very little upstream influence in the displacement. The transverse velocities are not shown here, but the field at the top of the lower deck, given by $\hat{D}(x,y)$, is not substantially affected by the stratification.

However, the transverse skin friction has waves which cause it to keep changing sign downstream; this destroys the secondary flow vortices of the homogeneous flow, see Figure 8 of (A).

Thus the buoyancy forces appear to generate waves confined to the downstream corridor, and also give slower asymptotic decay rates than the homogeneous flow.

4. The numerical model (two-dimensional)

For finite values of h_0, the lower deck equations (2.10) are non-linear, and must be solved numerically. For simplicity, we only consider two-dimensional flows, therefore V = 0, and there is no variation in the y-direction. Since separation in the triple-deck structure is a regular phenomenon, Stewartson (1974), a numerical model can be used to investigate separated flows, provided reverse velocities are not too large. Previous numerical work has often used an implicit Crank-Nicholson technique requiring a nonlinear relaxation at each step, e.g Smith (1974), Jobe and Burggraf (1974). .. A scheme for marching in the x-direction without iteration is presented below. The scheme is second - order accurate, and copes with reasonably separated flows without instability.

First, we apply a simple transformation to the lower-deck equations to give a horizontal lower boundary. Define

$$\left.\begin{aligned} Z' &= Z - h(x) \\ W' &= W - U\frac{dh}{dx} \end{aligned}\right\} \quad (4.1)$$

Substituting (4.1) into the equations (2.10) simply replaces Z by Z' and W by W'. So dropping primes, but remembering we are working in the

transformed variables, we have to solve

$$u\frac{\partial u}{\partial x} + W\frac{\partial u}{\partial Z} = -\frac{dP}{dx} + \frac{\partial^2 u}{\partial Z^2}$$
$$\frac{\partial u}{\partial x} + \frac{\partial W}{\partial Z} = 0 \qquad (4.2)$$

with boundary conditions

$$U = W = 0 \quad \text{at} \quad Z = 0$$
$$u \sim Z + A + h$$
$$W \sim -(Z + A + h)\frac{d}{dx}(A + h) \quad \text{as} \quad Z \to \infty$$

The solution method is to guess a displacement field, and, integrate (4.2) through the domain to obtain a pressure field. A new displacement can then be calculated in wavenumber space from (2.19), and the process continues until the change in the displacement is sufficiently small.

Equations (4.2) are integrated by finite - difference methods, using a uniform grid, with spacing δx and δz in the x- and z-directions respectively. Let u_{ij} denote the horizontal component of velocity at the point $(x_i, z_j) = ((i - \frac{M}{2})\,\delta x, (j-1)\,\delta z)$. We suppose that velocity values $u_{ij}, u_{i-1,j}$ are known for $j = 1$ to N then the values $u_{i+1,j}$ are obtained by a three stage process as described below.

Stage 1

Define $u_{i-\frac{1}{2},j} = \frac{1}{2}(u_{i-1,j} + u_{ij})$, then write the momentum equation as

$$\frac{u_{ij}}{\delta x}\left(\tilde{u}_{i+\frac{1}{2},j} - u_{i-\frac{1}{2},j}\right) + \left(W_{i,j-\frac{1}{2}} + \frac{\delta z}{2\delta x}\left(u_{i-\frac{1}{2},j} - \tilde{u}_{i+\frac{1}{2},j}\right)\right)\frac{(u_{i,j+1} - u_{i,j-1})}{2\delta z}$$
$$= -\tilde{G}_i + \frac{1}{\delta z^2}\left(u_{i,j+1} - u_{i-\frac{1}{2},j} - u_{i+\frac{1}{2},j} + u_{i,j-1}\right) \qquad (4.3)$$

where $\tilde{u}_{i+\frac{1}{2},j}$ is the first estimate of the advanced velocities at $x_{i+\frac{1}{2}}$, and $\tilde{G}_i$ is the estimated pressure gradient at the point i, which is to be calculated. Note that the viscous term in (4.3) uses the Du Fort - Frankel representation because of

unconditional instability of the explicit form. The vertical velocities can be calculated from the finite difference form of the continuity equation

$$W_{i,j-\frac{1}{2}} = \frac{\delta z}{\delta x} \sum_{r=2}^{j-1} \left(U_{i-\frac{1}{2},r} - \tilde{U}_{i+\frac{1}{2},r} \right) \qquad (4.4)$$

The boundary conditions on U_{ij} are applied in the obvious manner, i.e.

$$U_{i,1} = 0$$

$$U_{i,N} = (N-1)\delta z + A_i + h(x_i)$$

where A_i is the value of A at x_i.

The boundary condition W at $Z_{N-\frac{1}{2}}$ determines the pressure gradient $\tilde{G}_i$. Equation (4.3) is linear in $\tilde{U}_{i+\frac{1}{2},j}$, so first ignore the pressure gradient term, and advance the velocities, obtaining the values $U^*_{i+\frac{1}{2},j}$, say. Then calculate β_j, $j = 2, N-1$ such that

$$\tilde{U}_{i+\frac{1}{2},j} = U^*_{i+\frac{1}{2},j} - \beta_j \tilde{G}_i \qquad (4.5)$$

and choose the value of $\tilde{G}_i$ which gives

$$W_{i,N-\frac{1}{2}} = -\left((N-\tfrac{3}{2})\delta z + A_i + h(x_i)\right)\left(\frac{A_{i+1} - A_{i-1}}{2\delta x} + h'(x_i)\right) \qquad (4.6)$$

It can be shown that

$$\beta_2 = 1 \Big/ \left(\frac{1}{\delta z^2} + \frac{U_{i,2}}{\delta x} - \frac{U_{i,3}}{2\delta x} \right)$$

and

$$\beta_j = \frac{2\delta x + (U_{i,j+1} - U_{i,j-1}) \sum_{r=2}^{j-1} \beta_r}{2\delta x/\delta z^2 + 2U_{ij} - (U_{i,j+1} - U_{i,j-1})}, \quad j > 2.$$

Then

$$\tilde{G}_i = \frac{\left(W_{i,N-\frac{1}{2}} - W^*_{i,N-\frac{1}{2}} \right)}{\frac{\delta z}{\delta x} \sum_{r=2}^{N-1} \beta_r}$$

where $W_{i,N-\frac{1}{2}}$ is defined by (4.6), and $W^*_{i,N-\frac{1}{2}}$ is obtained from the continuity equation (4.4) using $U^*_{i+\frac{1}{2},j}$ for the advanced velocity. Having obtained , substitution in (4.5) gives the values of $\tilde{U}_{i+\frac{1}{2},j}$

Stage 2

In this stage, the velocities $\tilde{u}_{i+\frac{1}{2},j}$ are used to obtain a first guess for the velocities at x_{i+1}, i.e. $\tilde{u}_{i+1,j}$. This stage is almost identical to Stage 1, but is shifted by half a grid-length in the x-direction. We therefore only present the momentum equation.

$$\frac{\tilde{u}_{i+\frac{1}{2},j}}{\delta x}\left(\tilde{u}_{i+1,j}-u_{ij}\right)+\left\{w_{i+\frac{1}{2},j-\frac{1}{2}}+\frac{\delta z}{\delta x}\left(u_{ij}-\tilde{u}_{i+1,j}\right)\right\}\frac{\left(\tilde{u}_{i+\frac{1}{2},j+1}-\tilde{u}_{i+\frac{1}{2},j-1}\right)}{2\delta z}$$
$$=-\tilde{G}_{i+\frac{1}{2}}+\frac{1}{\delta z^2}\left(\tilde{u}_{i+\frac{1}{2},j+1}-\tilde{u}_{i+1,j}-u_{ij}+\tilde{u}_{i+\frac{1}{2},j-1}\right) \qquad (4.8)$$

Stage 3

This is the final stage, which uses the velocities from Stage 2 to produce the values of $u_{i+1,j}$. The viscous terms are treated implicitly in this stage, since the Du Fort - Frankel scheme tends to produce oscillatory solutions in the vertical.

Write the momentum equation in the form

$$\frac{\hat{u}_{i+\frac{1}{2},j}}{\delta x}\left(u_{i+1,j}-u_{ij}\right)+\frac{\hat{w}_{i+\frac{1}{2},j}}{4\delta z}\left(u_{i+1,j+1}+u_{i,j+1}-u_{i+1,j-1}-u_{i,j-1}\right) \qquad (4.9)$$
$$=-G_{i+\frac{1}{2}}+\frac{1}{2\delta z^2}\left(u_{i+1,j+1}+u_{i,j+1}-2u_{i+1,j}-2u_{ij}+u_{i+1,j-1}+u_{i,j-1}\right)$$

where $\hat{u}_{i+\frac{1}{2},j}=\frac{1}{2}\left(\tilde{u}_{i+1,j}+u_{ij}\right)$; $\hat{w}_{i+\frac{1}{2},j}=\frac{\delta z}{\delta x}\left\{\sum_{r=2}^{j-1}\left(u_{ir}-\tilde{u}_{i+1,r}\right)+\frac{1}{2}\left(u_{ij}-\tilde{u}_{i+1,j}\right)\right\}$

and $G_{i+\frac{1}{2}}$ is the pressure gradient, which is still to be determined.

Note that in this stage, vertical velocities are calculated explicitly from the previously estimated fields. However, we choose $G_{i+\frac{1}{2}}$ to make the final vertical velocity

$$w_{i+\frac{1}{2},N-\frac{1}{2}}=\frac{\delta z}{\delta x}\sum_{r=2}^{N-1}\left(u_{ir}-u_{i+1,r}\right) \qquad (4.10)$$

satisfy the upper boundary condition.

If we write (4.9) in matrix notation as

$$A\,\underset{\sim}{u}=-G_{i+\frac{1}{2}}\,\underset{\sim}{a}+\underset{\sim}{b}$$

where $\underset{\sim}{u} = (u_{i+1,2}, \ldots, u_{i+1,N-1})$, $\underset{\sim}{a} = (1,1,\ldots,1)$, A is a tri-diagonal matrix, and $\underset{\sim}{b}$ contains all the explicit terms in (4.9), then the solution is

$$\underset{\sim}{u} = A^{-1}\underset{\sim}{b} - G_{i+\frac{1}{2}} A^{-1}\underset{\sim}{a} \qquad (4.11)$$

This is precisely analogous to (4.5) in Stage 1, and since A is easily inverted, the pressure gradient can be determined from the boundary condition on vertical velocity, $W_{i+\frac{1}{2},N-\frac{1}{2}}$. The value of $G_{i+\frac{1}{2}}$ is then used to advance the pressure field.

After completing the sweep through to x_M, a new pressure field has been calculated. By means of the FFT routine, this is numerically transformed, and hence, using (2.19), a new displacement field is calculated. The adjustment of the displacement is under-relaxed, i.e.

$$A_i^{(new)} = (1-\varepsilon) A_i^{(old)} + \varepsilon A_i^{(calc)}$$

where $A_i^{(calc)}$ is the displacement value obtained from the latest pressure field, and $0 \leq \varepsilon < 1$. This procedure is necessary to prevent divergence in the displacement values, see Jobe and Burggraf (1974). The value of ε is adjusted automatically to maintain the maximum rate of convergence. The iteration is terminated when

$$\max_i \left| A_i^{(calc)} - A_i^{(old)} \right| < 5 \times 10^{-3} \max_i \left| A_i^{(old)} \right| .$$

For simplicity, periodic boundary conditions are specified in the x-direction, so the final values obtained at the end of a sweep become the starting values for the next sweep.

Note that the mean value of A is not determined by (2.19), since any constant can be added to the pressure field. The mean

value was adjusted during the iteration procedure to ensure that the pressure returned to its upstream value at x_M .

In order to deal with separated flows, it is assumed that the horizontal advection is negligible in reversed flow regions, the Reyhner - Flügge - Lotz (1968) approximation, so the first terms in equations (4.3), (4.8), (4.9) are set to zero in such regions. It is the problem of separation which necessitates the use of two initial estimates of the advanced velocities. The explicit calculation tends to produce oscillations in the x-direction with a wavelength of $2\delta x$, but taking two such steps seems to maintain the phase of this oscillation, and prevents it growing. This allows relatively strong separations to be calculated without signs of instability.

5. Numerical results

We first present a solution for homogeneous flow over the ridge

$$h(x) = \begin{cases} h_0 (1-x^2)^2 & , |x|<1 \\ 0 & , |x| \geq 1 \end{cases}$$

which will be the shape used in all the integrations presented in this section. Figure 5(a) shows streamlines of the lower deck flow with $h_0 = 3$, and the surface pressure and skin-friction appear in Figures 5(b) and (c). Only the central part of the domain of integration is shown, i.e. $|x| \leq 4$, $Z - h(x) \leq 12$, whilst the range used in the calculation is

$$-10 \leq x \leq 10 \ , \quad 0 \leq Z - h(x) \leq 15 .$$

Note that Z is the original Cartesian coordinate rather than the transformed variable. The solution shows an appreciable separation bubble behind the obstacle, and a corresponding reduction in the adverse pressure gradient in this region. The regularity of the separation is demonstrated by the smooth behaviour of the pressure and skin friction.

There is a small oscillation associated with the maximum reversed velocity evident in these figures, but this can be reduced by increased resolution, and does not have any significant effect on the solution. The general form of the solution is similar to that of linearized analysis, but the magnitude is slightly larger than might be expected. The flow first separates at $h_0 \simeq 1.9$, whereas extrapolation from the linear result implies the critical height is about 2.4.

Figures 6 and 7 illustrate the streamlines for the same hill, but with S = 3, and S = 5 respectively. It can be seen that when S = 3 the separation is completely suppressed, but S = 5 gives a similar result to the homogeneous case. (The minimum skin friction value achieved for the flow in Figure 6 is 0.1 at the rear of the hill.) There is evidently a type of resonant response when the natural wave-length, $\frac{2\pi}{S}$, is near to the length of the topography as is the case in Figure 6. The waves produced are then of large amplitude, and in phase with the hill, so the flow tends to remain attached. When S = 5, very little gravity wave energy is excited, and the streamlines are similar to those in Figure 5(a).

The solutions described above show that the presence of stable stratification in the free-stream can have a signficiant effect on the flow near the surface. Figure 8 shows the flow with S = 2 and where the wave amplitude is sufficient to induce a separation bubble downstream of the hill. This is a similar phenomenon to the 'rotors' generated by trapped lee-waves, e.g Long (1955).

The length of the domain of integration has been varied to ensure that the periodic boundary conditions do not have a significant effect

on the solution, and a length of 20 was found to be sufficiently long for all the flows described here. Most of the solutions converged within about 20 sweeps through the mesh, although the higher values of h_0 and S tended to take longer

6: Forces due to the hill

The total change in momentum transfer between the free-stream and the surface is the quantity of interest in meteorological applications. This is the sum of the pressure force on the hill and the change in total viscous force on the surface.

We consider the two-dimensional case, and use the transformation described in §4 i.e.

$$Z' = Z - h(x)$$
$$W' = W - U\frac{dh}{dx}$$

Write the momentum equation in the form

$$\frac{\partial}{\partial x}(U^2) + \frac{\partial}{\partial Z'}(UW') = -\frac{dP}{dx} + \frac{\partial^2 U}{\partial Z'^2} \qquad (6.1)$$

Integrating (6.1) over all values of x gives

$$\frac{\partial F_v}{\partial Z'} = \frac{\partial}{\partial Z'}\left[\int_{-\infty}^{\infty} UW'\,dx\right] \qquad (6.2)$$

where $F_v(Z') = \int_{-\infty}^{\infty}\left(\frac{\partial U}{\partial Z'} - 1\right)dx$, so $F_v(0)$ is the change in viscous drag on the surface.

The other terms in (6.1) vanish upon integration since $P \to 0$ as $x \to \pm\infty$ and the velocity perturbations decay too rapidly downstream for a momentum-deficit to be maintained.

Integrating (6.2) from $Z' = 0$ to infinity gives

$$F_v(0) = -\lim_{Z'\to\infty}\int_{-\infty}^{\infty} UW'\,dx \qquad (6.3)$$

Using the upper boundary condition on W', and the equations of motion, asymptotic expansions for U, W' valid for $Z' \to \infty$ can be obtained. These are

$$U \sim Z' + A + h + O(Z'^{-3})$$
$$W \sim -Z\frac{d}{dx}(A+h) - (A+h)\frac{d}{dx}(A+h) - \frac{dP}{dx} + O(Z'^{-2})$$

So substituting in (6.3) gives

$$F_v(0) = -\int_{-\infty}^{\infty}\left(P\frac{dh}{dx} + P\frac{dH}{dx}\right)dx$$

Hence the total force on the surface, after adding the pressure force, is

$$F = \varepsilon^4 \bar{\rho} U_0^2 L \int_{-\infty}^{\infty} P \frac{dA}{dx} dx \qquad (6.4)$$

This is precisely the force due to inviscid flow over the topography $-A(x)$, since $P(x)$ is the pressure at the bottom of the upper deck. The only mechanism capable of producing a force in such a flow is the radiation of energy to infinity by gravity waves. Thus the total force on the surface is changed only by the gravity wave drag.

The analysis can be carried out in three-dimensional flows, although the algebra is more complicated, and gives a similar result, i.e. the only extra momentum transfer is due to wave radiation.

The variation of the drag with S for small hills can be calculated from the linear theory. The results for the ridge used in are illustrated in Figure 9. The graph shows a maximum wave drag when $S \doteq 3$, which is the value giving a natural wavelength the same length as the topography. For S small, the force grows roughly linearly, while for S large, it decreases like S^{-1}. This variation of wave drag with inverse Froude number is quite different to that of the inviscid, linear, wave-generation theory of Miles and Huppert (1969). The inviscid theory gives a force which continues to grow linearly with S, provided that the vertical Froude number $\varepsilon^2 S$, which is based on the height of the obstacle rather than its length, remains small. The reason for the difference is that for the inviscid flow there is no boundary layer, and the wave amplitude must be of the same order as the height of the topography. However, when the hill lies inside a viscous boundary layer there is a cushioning effect between the surface and the free-stream, and the displacement

at the top of the boundary layer is generally smaller than that at the surface. For higher values of S, the free-stream becomes more resistant to vertical displacement, and solution of the linearised equations shows that the amplitude of the streamline displacement, $\hat{A}$, decreases like S^{-1}, resulting in a reduction in force at large S.

The growth of the drag force with increasing h_o is shown in Figure 10. The results are obtained from the numerical model, using S = 2. The linear result is shown as the dashed line, which coincides with the numerical results for small h_o. However for $h_o > 1$, the force increases significantly faster than h_o^2; the slope of the graph is approximately 2.32. This is due to the fact that the amplitude of the waves grows like $h_o^{1.16}$; so for $h_o > 1$, the waves will be larger than predicted by linear theory.

The upper line in Figure 10 shows the wave drag predicted by inviscid linear theory, i.e. no boundary layer present. The height of the hill is $O(\varepsilon^2 L)$; therefore the linearisation is valid. The results are obviously quite different, due to the interaction with the boundary layer dynamics, and in this case, the inviscid theory predicts a larger drag for small values of h_o. However, since the triple deck results show the drag growing faster than h_o^2, the two curves will eventually cross, but for this particular hill the cross-over point will be at very large h_o.

6. Remarks

It has been shown that the presence of stable stratification in the free stream can have dramatic effects on the boundary layer flow. Within the framework of the triple deck analysis, it appears that

separation can be inhibited, and downstream rotors can be produced. Although the interaction with a turbulent boundary layer would probably be less strong, it seems likely that there would be a qualitative similarity. Such features in the flow near the surface could be of importance in the dispersion of pollutants near hills.

The gravity waves induced in the free stream are quite different in amplitude and shape to those predicted by an inviscid theory. Although the slope of the topography is asymptotically small, $O(\varepsilon^2 h_o)$, it is found that the wave amplitude increases like $h_o^{1.16}$. Effects such as this may be of importance in determining the amplitude of gravity waves in the atmosphere, since inviscid linear theories often seem inadequate, see e.g. R B Smith (1976).

Finally, I would like to express my thanks to Dr F T Smith for many helpful discussions of this work.

References

Bretherton, F.P (1969): 'Momentum transport by gravity waves' Q.J.Roy. Met. Soc. 95 p 213

Jobe, C.E. and Burggraf, O.R. (1974): 'The numerical solution of the asymptotic equations of trailing edge flow' Proc.Roy.Soc. A340 p 91

Long, R.R. (1955): 'Some aspects of the flow of stratified fluids. III Continuous density gradients.' Tellus 7 p 342

Miles, J.W. and Huppert, H.E. (1969): 'Lee waves in a stratified flow, Part 4. Perturbation approximations' J. Fluid Mech. 35 p 497

Queney, P. (1948): 'The problem of airflow over mountains: a summary of theoretical studies' Bull. Am. Met. Soc. 29 p 16

Reyhner, T.A. and Flügge-Lotz, I. (1968): 'The interaction of a shock wave with a laminar boundary layer' Int. J. Nonlinear Mech. 3 p 173

Scorer, R.S. (1953): 'Theory of airflow over mountains: II - The flow over a ridge' Q.J. Roy. Met. Soc. 79 p 70

Smith, F.T. (1973): 'Laminar flow over a small hump on a flat plate' J. Fluid Mech. 57 p 803

Smith, F.T. (1974): 'Boundary layer flow near a discontinuity in wall conditions' J. Inst. Math. Appl. 13 p 127

Smith, F.T. (1976): 'On entry flow effects in bifurcating, blocked or constricted tubes'. J. Fluid Mech. 78 p 709

Smith, F.T., Sykes, R.I., and Brighton, P.W.M. (1977): 'A two-dimensional boundary layer encountering a three-dimensional hump' to appear in J. Fluid Mech.

Smith, R.B. (1976): 'The generation of lee waves by the Blue Ridge' J. Atmos Sci. 33 p 507

Stewartson, K (1974): 'Multi-structured boundary layers on flat plates and related bodies' Advances in Appl.Mechs. 14 p 145 (Academic Press)

Figure captions

Figure 1 : Schematic diagram of flow geometry and coordinate system.

Figure 2 : Contours of the linearised pressure solution, $\hat{P}$. The square illustrated is $|x| \leqslant 7.5$, $|y| \leqslant 7.5$, and the topography is given in equation (3.1). The contour interval is 0.02, and solid contours denote positive values, dashed contours negative values.

Figure 3 : Contours of the linearised skin-friction pertubation $\left.\frac{\partial \hat{U}}{\partial Z}\right|_{Z'=0}$

The contour interval is 0.1.

Figure 4 : Contours of the linearised streamline displacement solution, $-\hat{A}$. The contour interval is 0.02, and positive values imply upward displacement.

Figure 5 : (a) Streamlines from numerical solution with $h_0 = 3$, $S = 0$, $\delta x = 0.08$, $\delta z = 0.25$, $M = 256$, $N = 60$. The domain illustrated is $|x| \leqslant 4$, $Z - h(x) \leqslant 12$.

(b) Grid-point values of dimensionless pressure P for $h_0 = 3$, $S = 0$.

(c) Grid-point values of skin friction, $\left.\frac{\partial U}{\partial Z}\right|_{Z'=0}$

Figure 6 : Streamlines for $h_0 = 3$, $S = 3$, other parameters as figure 5.

Figure 7 : Streamlines for $h_0 = 3$, $S = 5$, other parameters as figure 5.

Figure 8 : Streamlines for $h_0 = 6$, $S = 2$, $\varkappa = 0.5$, other parameters as figure 5. Domain illustrated is $|x| \leqslant 6$, $Z - h(x) \leqslant 24$.

Figure 9 : Graph of linearised wave drag, $\frac{F}{\varepsilon^4 h_0^2 \bar{\rho} U_0^2 L}$, against S.

Figure 10: Graph of dimensionless wave drag $\frac{F}{\varepsilon^4 \bar{\rho} U_0^2 L}$, against h_0.

Numerical results are represented by crosses.

– – – – represents results from the linear theory.

—· —· — represents results from inviscid linear theory.

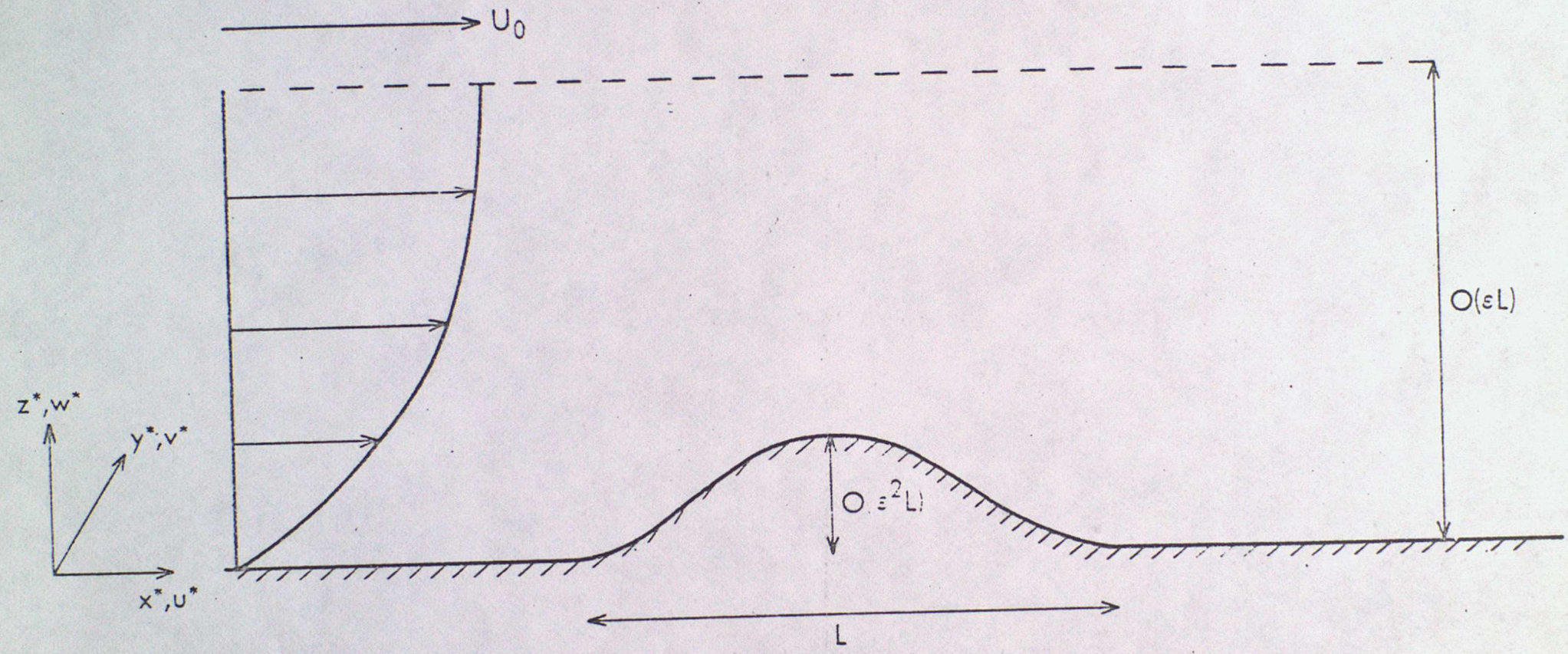

Fig 1

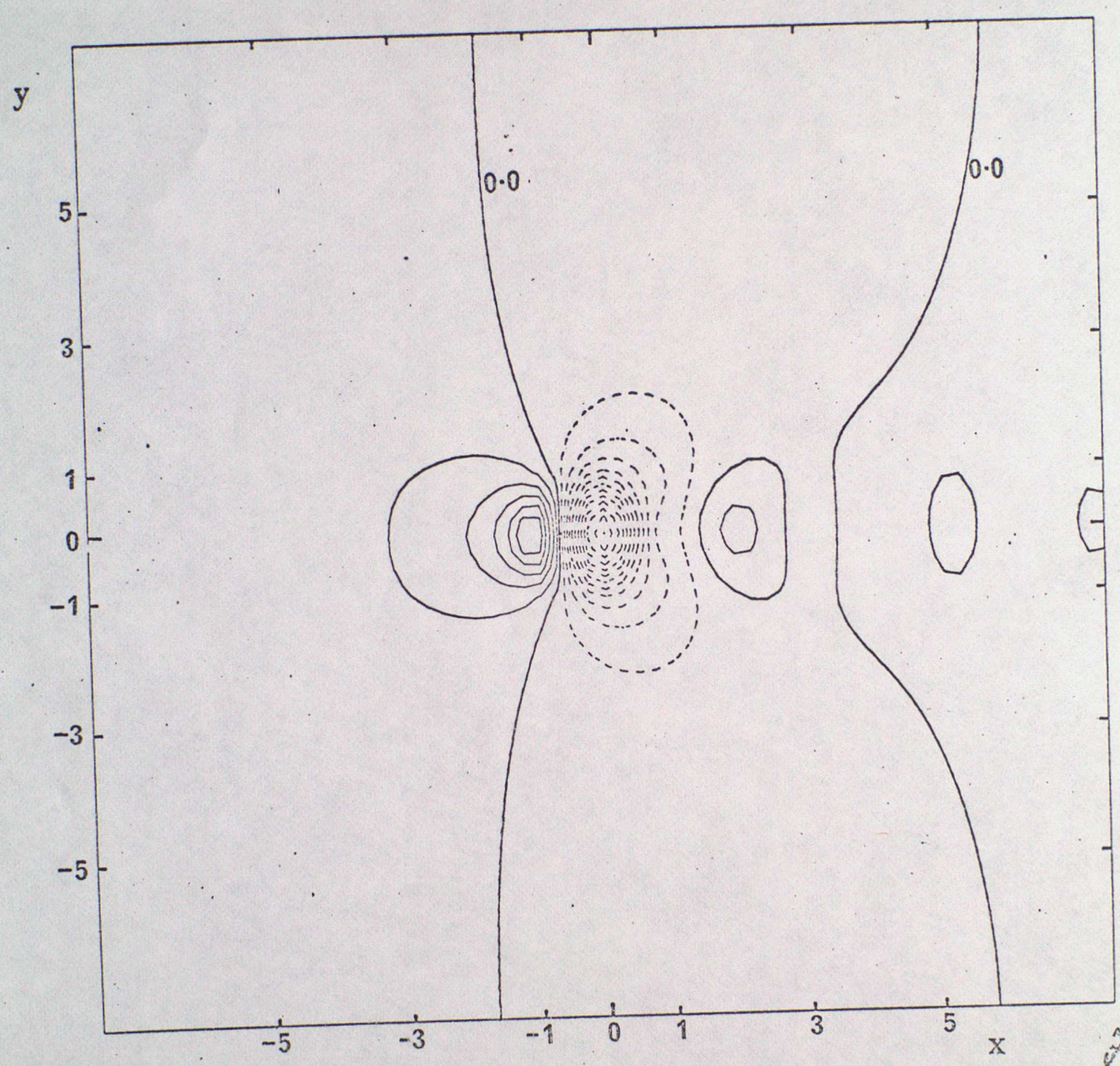

Fig 2

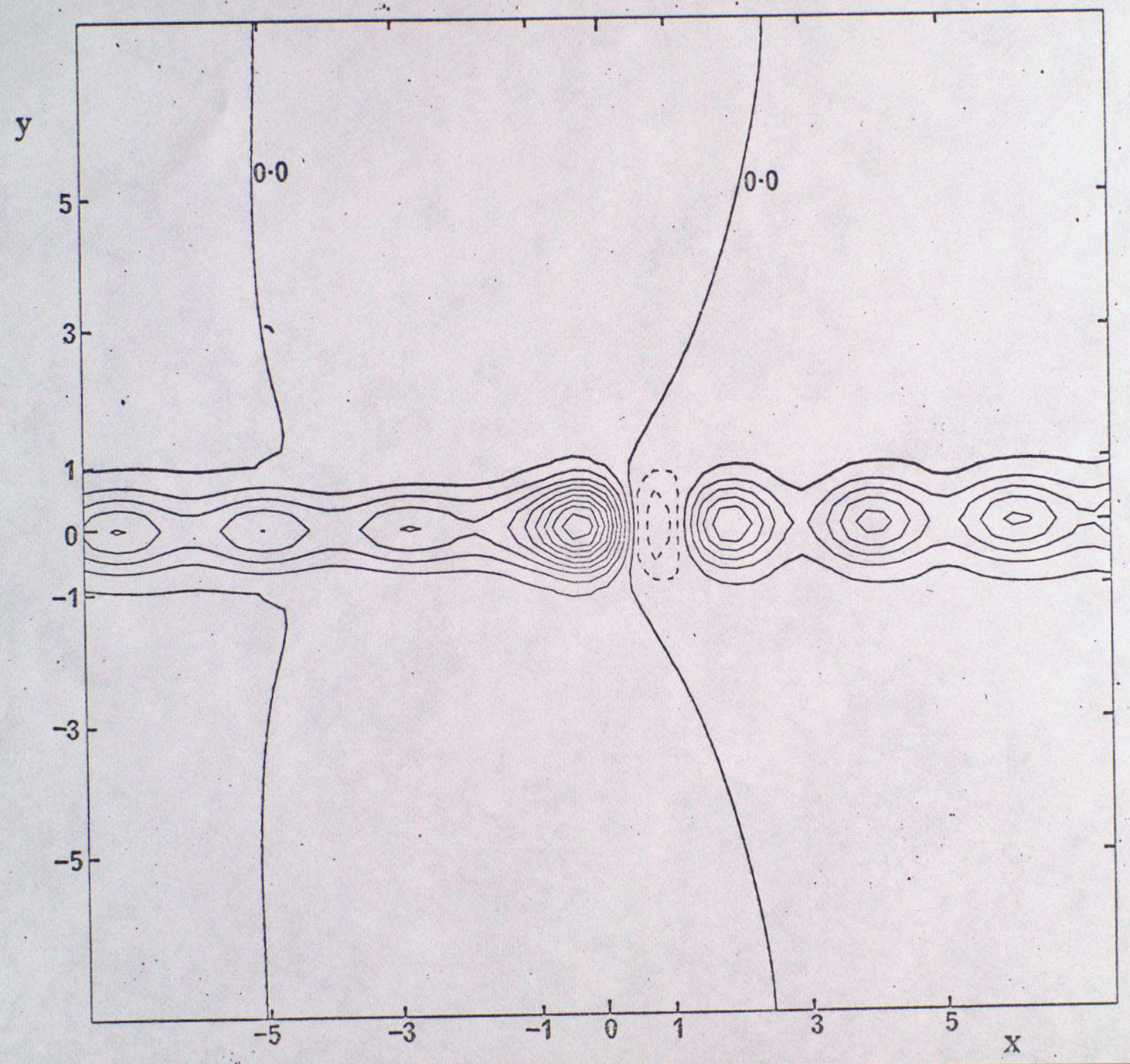

Fig 3

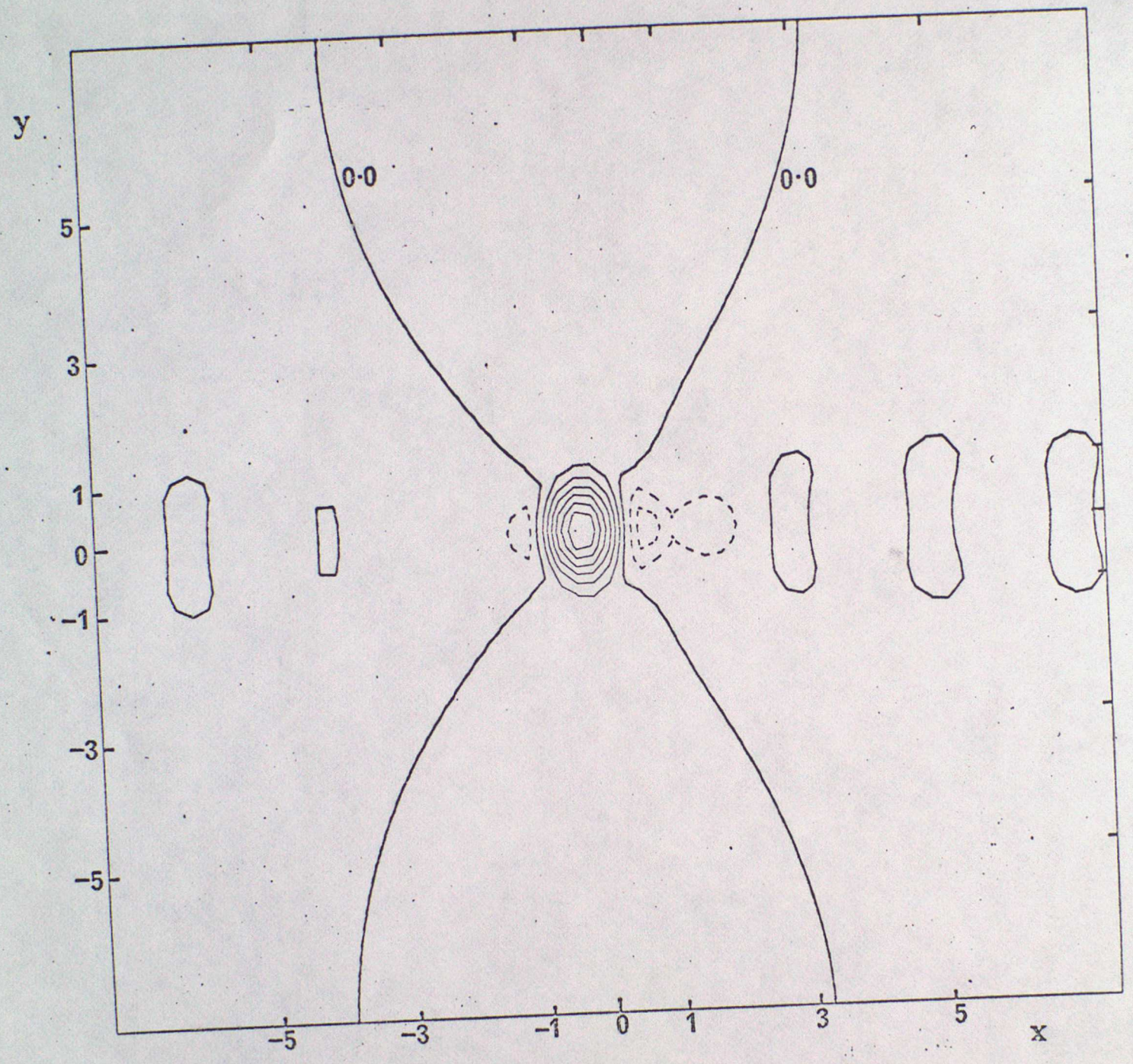

Fig 4

Fig. 5(a)

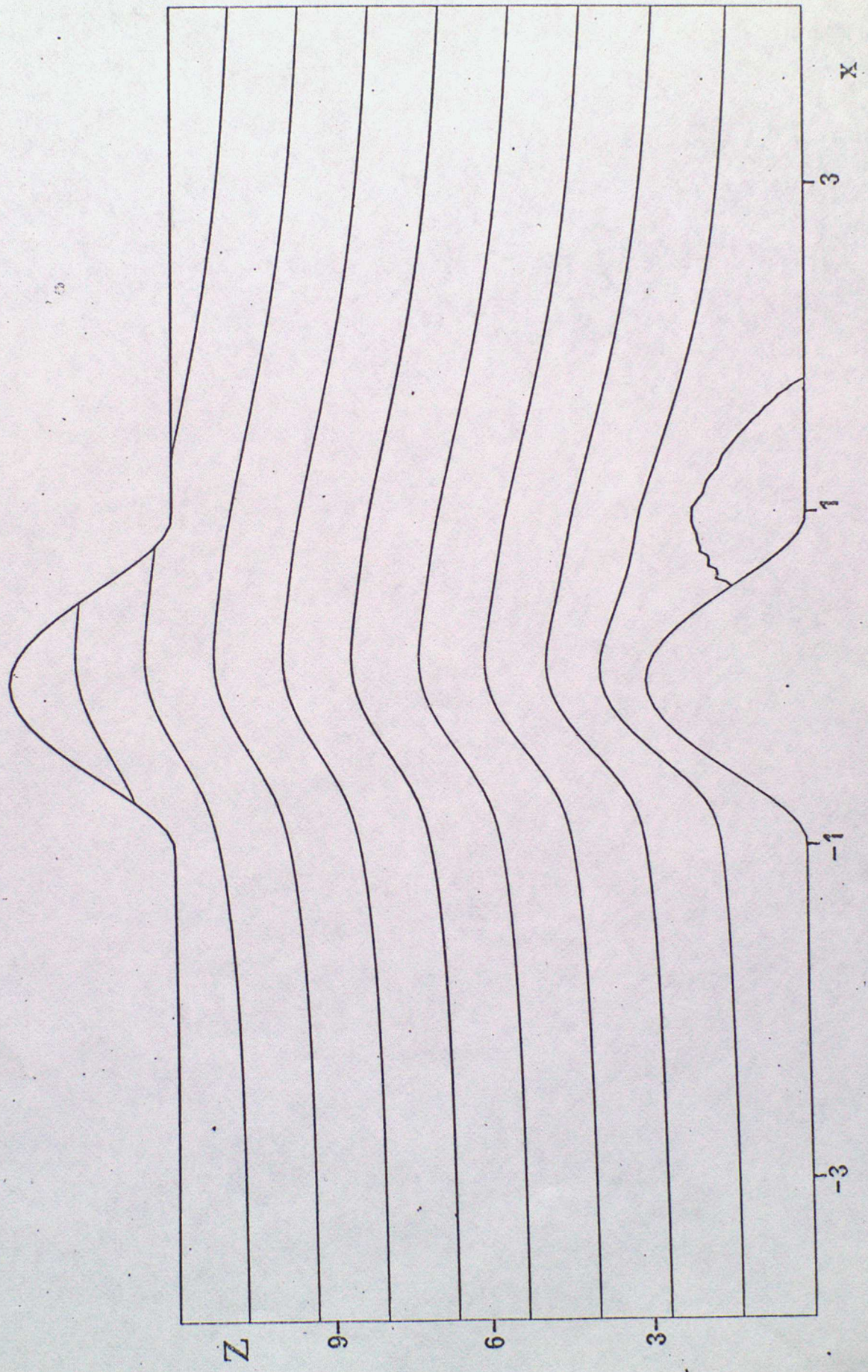

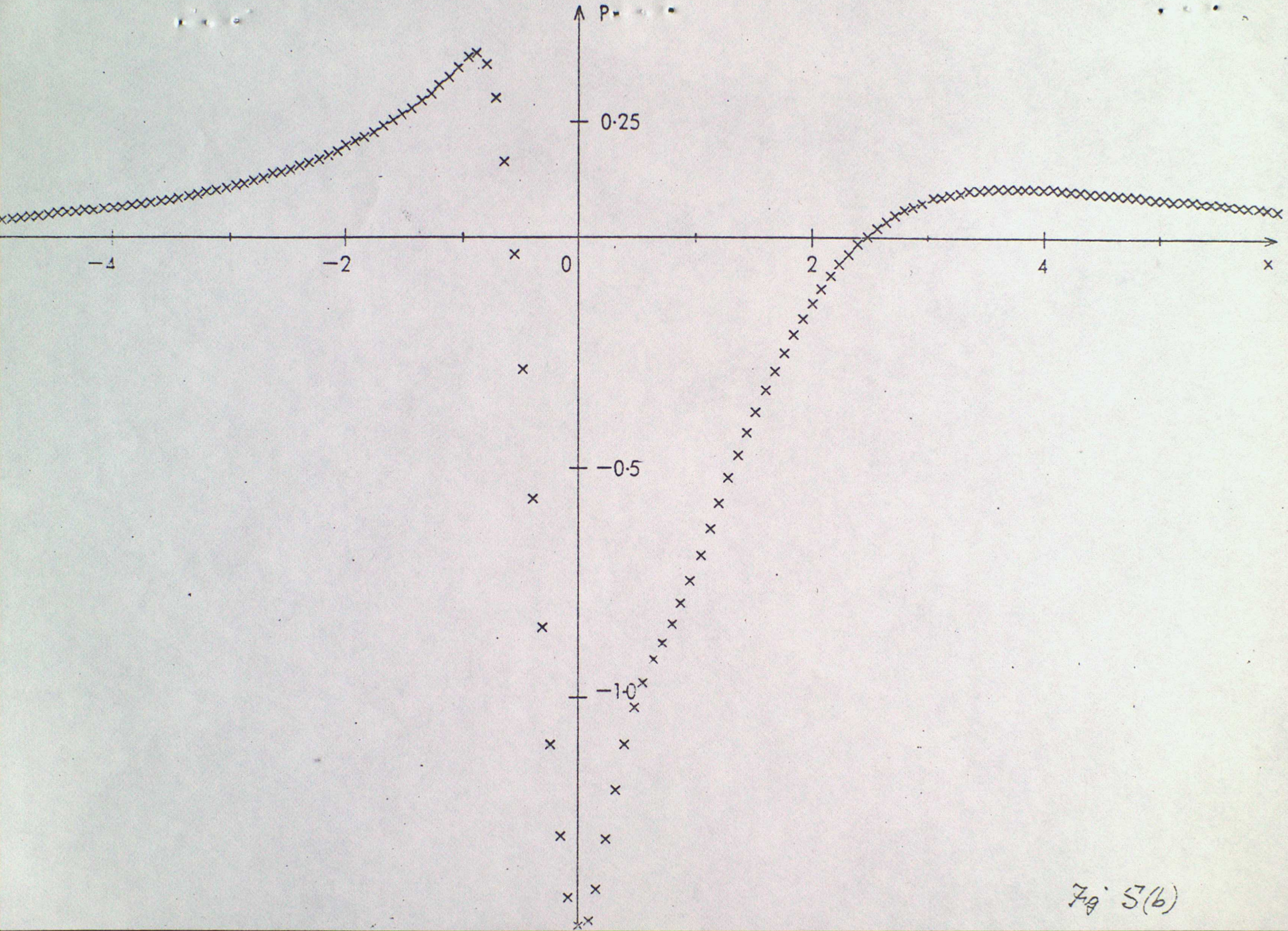

Fig. 5(b)

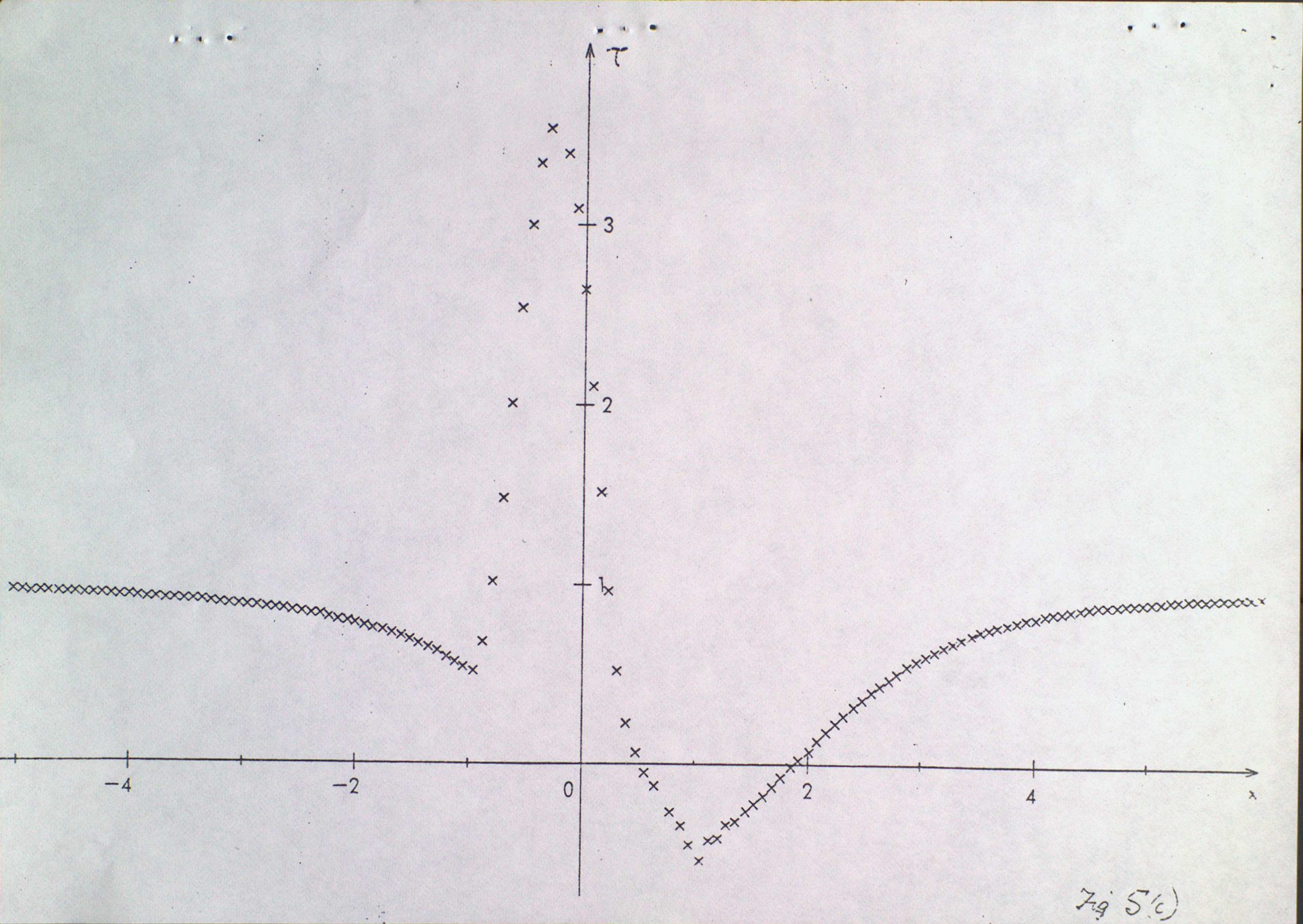

Fig 5(c)

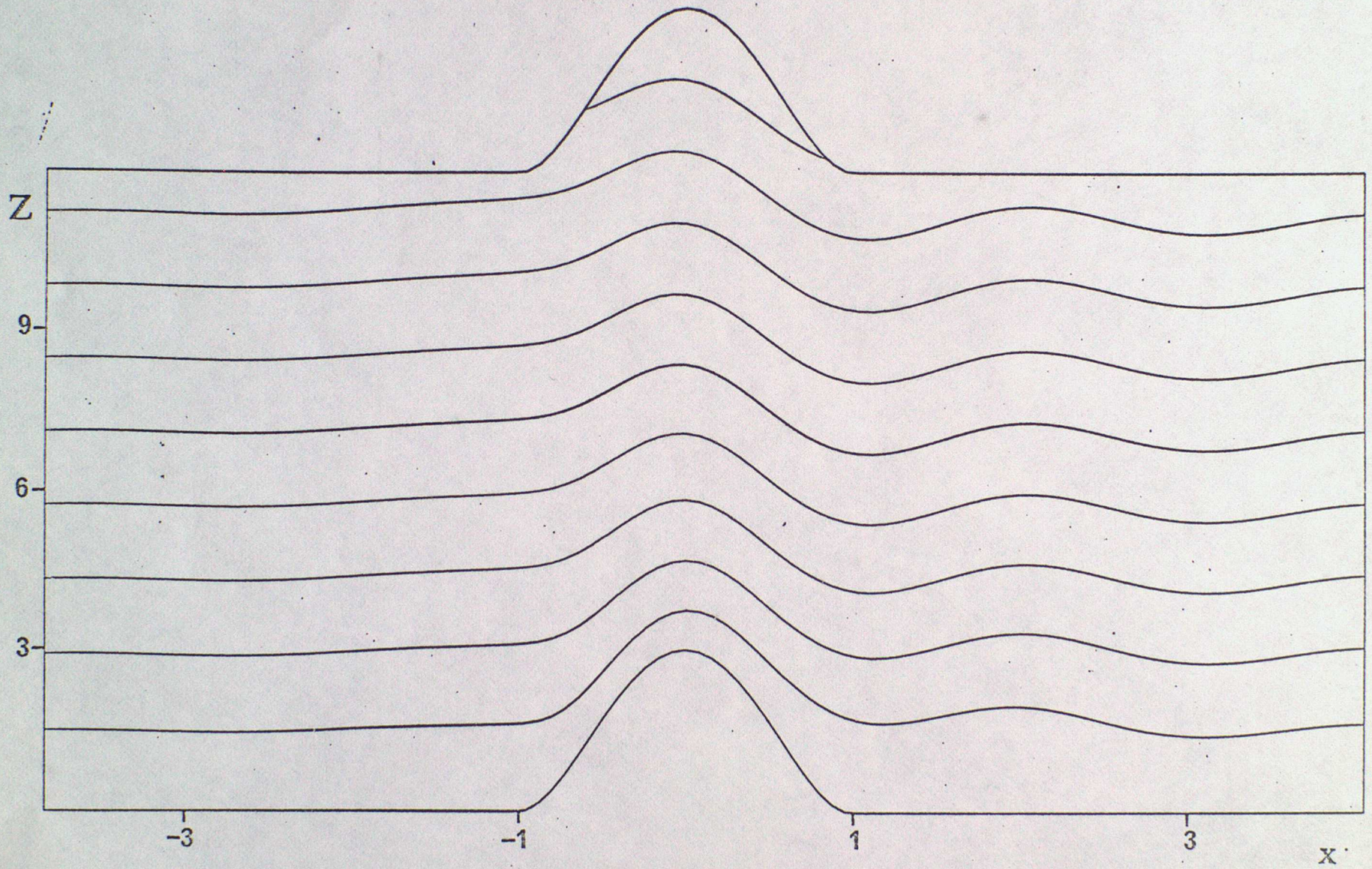
Z
9
6
3
-3
-1
1
3
x

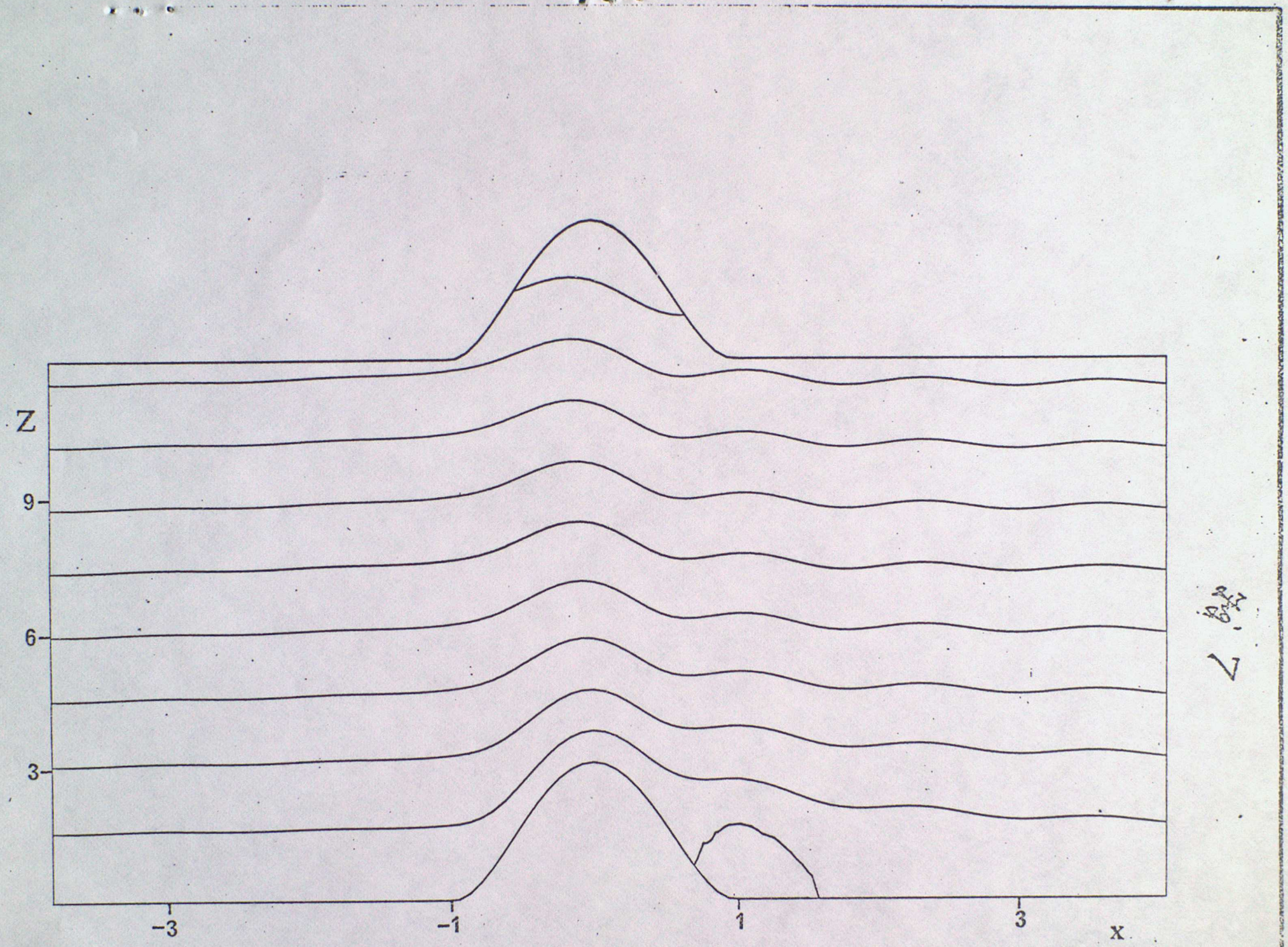
Z
9
6
3
−3
−1
1
3
x

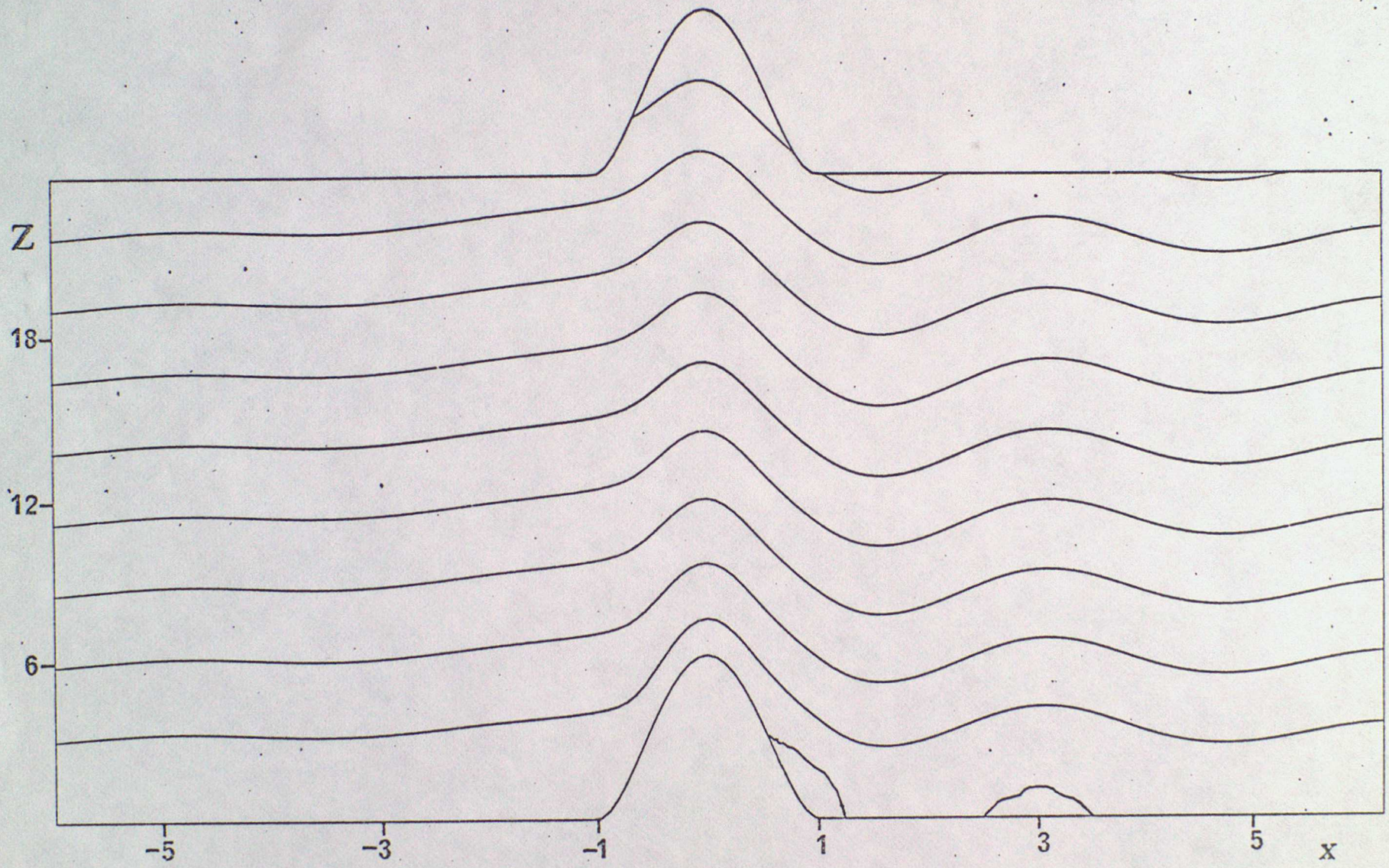
Z
18
12
6
-5
-3
-1
1
3
5
x

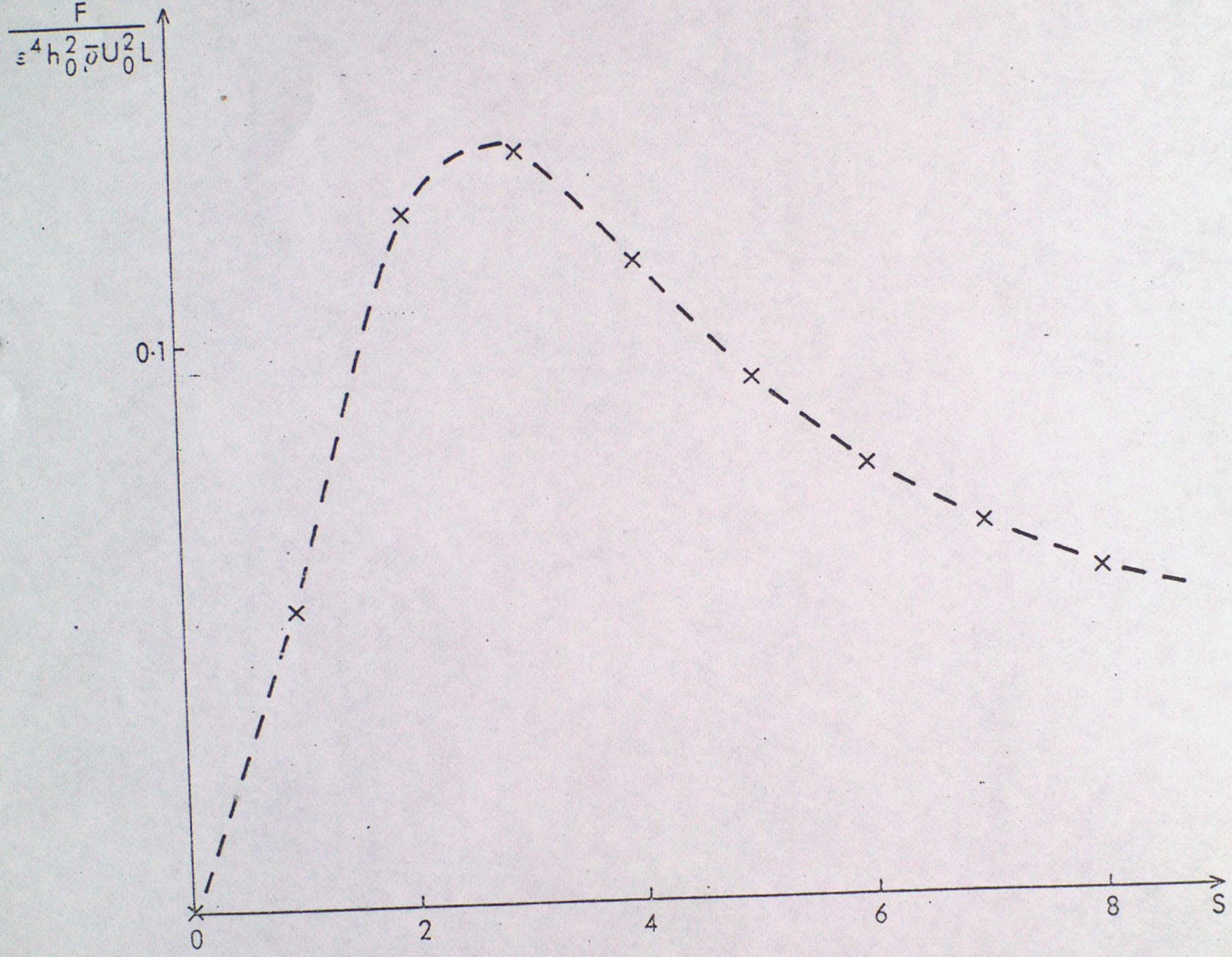

Fig 9

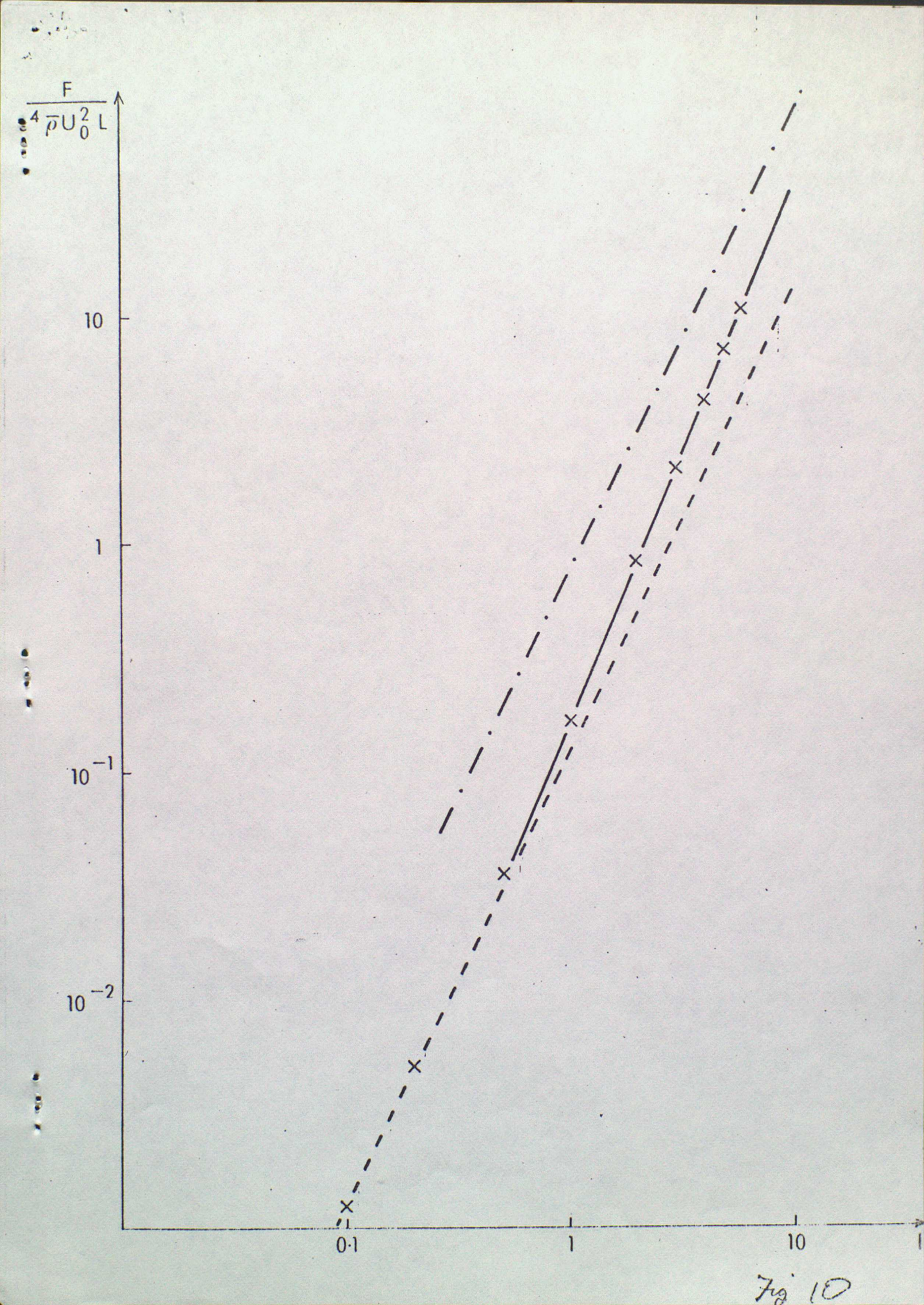

Fig 10